SCIENTIFIC REPORTS

OPEN

SUBJECT AREAS:
MAGNETIC PROPERTIES AND MATERIALS
FERROMAGNETISM

Received
11 June 2014

Accepted
8 August 2014

Published
27 August 2014

Correspondence and requests for materials should be addressed to J.R.S. (jrsun@iphy.ac.cn)

* These authors contributed equally to this work.

# Anomalous magnetism in strained $La_{1-x}Sr_xCoO_3$ epitaxial films ($0 \leq x \leq 0.5$)

H. W. Yang[1]*, H. R. Zhang[1,2]*, Y. Li[1], S. F. Wang[2], X. Shen[1], Q. Q. Lan[1], S. Meng[1], R. C. Yu[1], B. G. Shen[1] & J. R. Sun[1]

[1]Beijing National Laboratory for Condensed Matter & Institute of Physics, Chinese Academy of Sciences, Beijing 100190, People's Republic of China, [2]College of Physics Science and Technology, Hebei University, Baoding 071002, Hebei Province, People's Republic of China.

**Spin state controlling has always been a focus of intensive studies due to its importance for novel effect exploration and information technology. Complex oxides with competitive mechanisms are suitable objects of study for this purpose due to their susceptibility to external stimuli. Perovskite cobaltate $La_{1-x}Sr_xCoO_3$ is one of such oxides. Combined effects of lattice strains and hole-doping have been studied for the LSCO films with $0 \leq x \leq 0.5$. It is found that the lattice strain, either tensile or compressive, destabilizes the ferromagnetic (FM) state of the epitaxial films, leading to a nonmagnetic state that extensively exists in a doping window embedding deep into the range of the FM phase in bulk counterparts. Density functional theory calculations reveal a distinct spin state transition due to the combined effects of lattice distortion and hole-doping, explaining the unique magnetic behaviors of LSCO.**

Spin state manipulation has always been a focus of intensive studies due to its importance for novel effect exploration and information technology. Complex oxides with competitive mechanisms are suitable objects of study for this purpose due to their susceptibility to external stimuli. Perovskite cobaltate $LaCoO_3$ (LCO) is one of such oxides[1–10]. A typical phenomenon observed in LCO is spin state transition. With the increase of temperature, as well documented in literature, $Co^{3+}$ ions which are initially in a low spin state (LS, $t_{2g}^6 e_g^0$, $S=0$)[3–8] gradually transit into an intermediate spin state (IS, $t_{2g}^5 e_g^1$, $S=1$) above 35 K[3–6], to a IS and a high spin (HS, $t_{2g}^5 e_g^1$, $S=2$) mixed state above 300 K, and to the HS state above 550 K[3,5]. In addition to thermal energy, lattice strain also strongly affects the spin state of LCO[10–17]. It was recently found that the $Co^{3+}$ ions will take the HS state under tensile strains otherwise the LS state[10–12]. The population of the HS $Co^{3+}$ ions can also be tuned by tuning lattice strain, and a moment jump from 0 to ~0.8 $\mu_B$/Co can be realized by applying an in-plane tensile stress to LCO[11]. Therefore, if a technique that triggers lattice strain among different states can be found, the magnetic moment of LCO will be readily switched between definite values. This is the case demonstrated in a recent work by Hu *et al*[18]. Based on a delicately designed device, the authors showed that the ferromagnetic-nonmagnetic (FM-NM) transition repeats while cycling a gating field across the LCO/$SrTiO_3$ film.

LCO is a member of the $La_xSr_xCoO_3$ (LSCO) family. Its ground state is NM without being strained. An interesting question is what the strain effect will be for other members, particularly those that are originally in the FM state. We expect a distinct strain effect in LSCO for two reasons. At first, Sr doping brings about $Co^{4+}$ ions. This will modify the nature of the exchange coupling, converting the superexchange (SE) among $Co^{3+}$ ions in LCO[14,19] to double exchange (DE) between $Co^{3+}$ and $Co^{4+}$ ions[16]. Second, the presence of Sr leads to La-site disorder. The resulting inhomogeneous lattice distortions will amend crystal-field splitting, thus the spin state of Co ions[10–16]. We noticed that most of the previous works about strained LSCO films focused on two limiting cases of $x=0$ and 0.3[14,16,20,21], for which two completely different mechanisms, the SE and the DE, prevail, respectively. In intermediate doping range, the SE and DE could be in strong competition with each other, and a unique strain effect would be resulted when their balance is broken. Hopefully, studies in this regard would lead to a deep understanding on the magnetism in strained cobaltate, which has been a long-standing mystery[13–17], and lead us to a better control of the spin state of LSCO. In this letter, we report on a systematic study on the combined effects of lattice strain and hole-doping for the LSCO films ($0 \leq x \leq 0.5$). We found that lattice strain, particularly tensile strain, induces a NM to FM transition for LCO but a FM to NM transition for LSCO when the content of Sr is low,

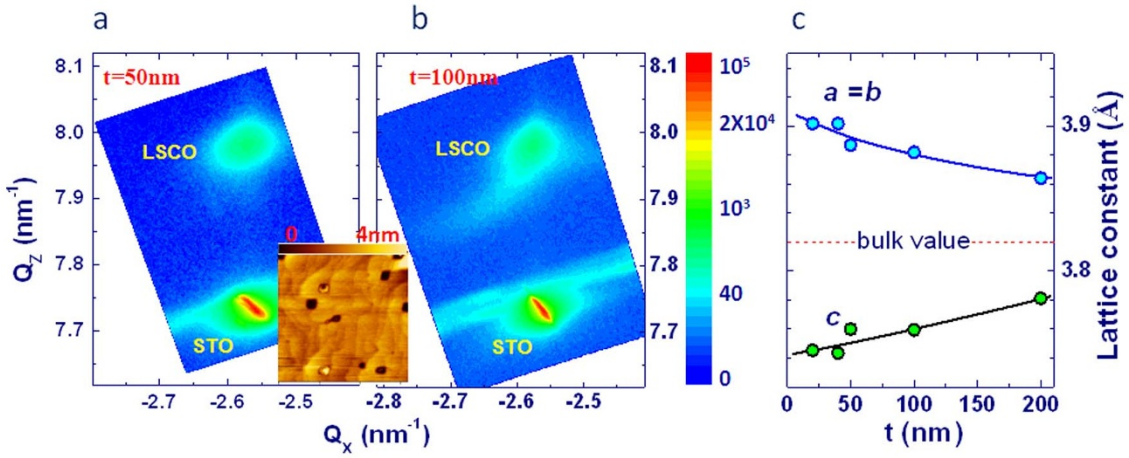


**Figure 1 | Crystal structure of the (001)-LSCO($x$=0.2)/STO films of different thicknesses.** (a) and (b) X-ray reciprocal space maps around the (-103) Bragg reflections of the LSCO/STO films with the thicknesses of 50 nm (a) and 100 nm (b). The inset plot is the topography of a 50-nm-thick LCO/STO film. Image size is 1 μm × 1 μm. (c) Lattice parameter of the LSCO/STO films, deduced form reciprocal space maps. Dashed line indicates the lattice constant of bulk LSCO.

with a moment drop as large as 0.8–1.1 μB/Co. The NM state exists in a wide doping window that penetrates deep into the region for the FM state of bulk LSCO. *Ab initio* calculations indicate that, with the help of lattice strain, the introduction of Sr triggers a HS to LS state transition of the $Co^{3+}$ ions, rather than the LS to IS transition as occurred in bulk LSCO. This weakens the FM coupling, leading to the NM state.

## Results and discussions

**Structure characterization.** The LCO film shows a terrace-featured morphology with a step height of 4 Å, indicating a two-dimensional film growth (inset in Fig. 1). Although the film surface becomes mosaic-like when $x$ is high (not shown), the surface undulation remains low (<6 Å). X-ray diffraction analysis shows that all films are well epitaxially grown on substrates. Fig. 1 is the representative reciprocal space mapping (RSM) of the (-103) reflection of the (001)-LSCO/STO film ($x$=0.2). The diffraction peak of the film locates right above that of the substrate when film is thin, i.e., the in-plane lattice parameter of the film is exactly that of the substrate. Based on the RSMs of the (-103) and (0–13) peaks, the lattice parameters can be deduced, and they are $a$=$b$=3.905 Å and $c$=3.745 Å for the 20-nm-thick film. This result indicates an in-plane tensile strain and an out-of-plane compressive strain in the film noting the bulk lattice constants of ~3.820 Å for bulk LSCO[22]. Thin LSCO films could be fully strained since the diffraction spot is symmetric (Figs. 1a). Considerable lattice relaxation occurs when film is thick, leading to a tadpole-like appearance of diffraction spot (Figs. 1b). As $t$ grows from 20 nm to 200 nm, $a$ or $b$ decreases from 3.905 to 3.864 Å, whereas $c$ increases from 3.745 to 3.781 Å. Notably, lattice strain is still substantial even in well relaxed 200-nm-thick film. Lattice strain is also detected in LSCO/LAO, though it is less significant because of the similar lattice parameters of LSCO and LAO.

To get further information about the mode for film growth and interface structure, we performed a transmission electron microscopy (TEM) analysis of the LSCO films. Fig. 2 illustrates the high angle annular dark-field (HAADF) images for two selected films LCO/STO and LSCO(x=0.1)/STO, acquired at the acceptance angles of 70–150 mrad. The HAADF images show a perfect epitaxial film growth on the substrate. The film is fully strained, and the film-substrate interface is very clear, free from interfacial defects. Similar to reported results[23,24], dark stripes perpendicular to interface are observed in the LCO films, appearing every other three or four columns, and the closest stripes are only 2–3 unit cells away from the interface. Some authors believed that the dark stripes are formed by HS $CoO_6$ octahedra[23], whereas others ascribed them to oxygen deficient regions and argued that the HS $Co^{2+}$ ions sandwiching the dark stripes are responsible for the ferromagnetism in LCO[24]. In any cases, the ferromagnetism appears accompanying the dark stripes. Fascinatingly, dark stripes disappear in the HAADF image of the LSCO film, and a fully strained and homogeneous structure is observed (Fig. 2(b)). As will be seen later, this result reflects a depression of the ferromagnetism in LSCO by the incorporation of minor Sr ions.

**Combined effects of lattice strain and hole doping.** Figs. 3a and 3b show the temperature-dependent magnetization, $M$-$T$, of the (001)-LSCO films with $t$=50 nm, measured with an applied field of 0.05 T in field-cooling mode. Similar to the previously reported results, the tensile LSCO/STO films of $x$=0 and $x \geq 0.3$ are in FM state at low temperatures, and the Curie temperature, defined by the inflection point in the $M$-$T$ curve, varies between 80 and 205 K. Fascinatingly, the FM character is greatly weakened in the intermediate doping range of $0.05 < x < 0.2$. As shown by the amplified $M$-$T$ curves the inset in Fig. 3a, the steep cliff for $x$=0 declines when $x$=0.05, and

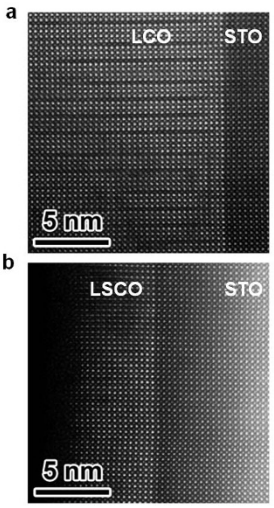


**Figure 2 |** (a) High angle annular dark-field (HAADF) image of the LCO/STO film with a thickness of 50 nm. (b) HAADF image of a 7-nm-thick LSCO(x=0.1)/STO film. Periodical dark stripes in the LCO film but not the LSCO film can be clearly seen.

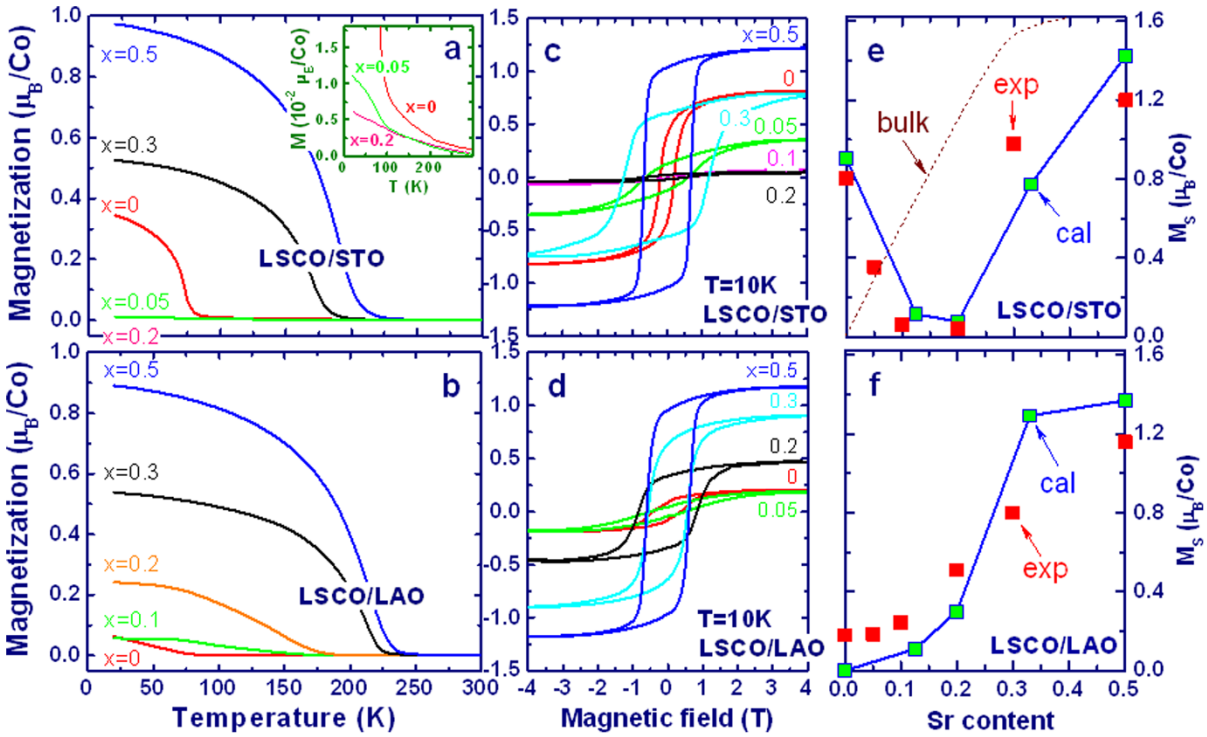


**Figure 3 | Doping effect on magnetism for the LSCO films grown on different substrates with a constant thickness of 50 nm.** (a) and (b) Thermal magnetizations of the LSCO/STO (a) and LSCO/LAO (b) films, recorded in the warming process after field cooling the films to 10 K. The applied field is 0.05 T. (c) and (d) Isothermal magnetizations of the LSCO/STO (c) and LSCO/LAO (d) films, recorded at 10 K. (e) and (f) Saturation magnetizations as functions of Sr content, deduced from the *M-H* curves in (c) and (d), respectively. Red/green symbols represent the observed/calculated results. Data of the bulk LSCO (extracted from Ref. 1) are shown in (e) by a dashed line.

disappears completely when $x$=0.2. The strong-to-weak crossover of the magnetic character is clearly shown by Fig. 3c: Different from the typical FM behavior of the films with $x$=0, 0.3, and 0.5, the *M-H* curves for $x$=0.1 and 0.2 are essentially NM in nature. According to Fig. 3e, the saturation magnetization, $M_S$, is only ~0.06 $\mu_B$/Co for $x$=0.1 and ~0.04 $\mu_B$/Co for $x$=0.2. These values are much lower than the corresponding bulk ones (dashed line in Fig. 3e)[1,2]. This implies that, by simply applying lattice strain, we can realize not only the NM→FM transition of LCO but also the FM→NM transition of LSCO for $x$<0.2. Obviously, the intertwined strain and doping effects make the FM state unstable. The magnetization rises again when $x$ exceeds 0.3, and approaches a saturation value. The magnetic behavior of the LSCO/LAO film is relatively simple. It is weakly FM for $x < 0.1$ and strongly FM for $x \geq 0.2$ (Fig. 3b). The $M_S$ grows monotonically from ~0.1 to ~1.2 $\mu_B$/Co as $x$ increases from 0 to 0.5, without any anomalies in the intermediate doping range (Figs. 3d and 3f). One thing deserving special attention is that the magnetization of the film is fairly lower than that of the bulk values even when $x > 0.3$, indicating the robustness of the strain effect.

To verify the unique strain effect in tensile films, thermal magnetization is measured for differently relaxed films. As a consequence of lattice strain, as shown in Fig. 4a, the magnetization of the LCO/STO film displays a monotonic decrease with $t$ when $t > 40$ nm. $M$ of the 20-nm-thick film is abnormally low $M$ (~0.22 $\mu_B$/Co), probably due to interfacial effect. In contrast, the FM state of the LSCO($x$=0.2)/STO film is increasingly enhanced by increasing $t$. As shown in Fig. 4b, the magnetization is nearly zero for $t$=20 nm, and remains low until film thickness exceeds 50 nm. However, it undergoes a 50-fold growth from $t$=50 nm to 200 nm. Obviously, with the release of lattice strain, the FM order is deteriorated in LCO but rebuilt in LSCO.

To quantify the strain effect, the $M_S$-$\sigma$ dependences are studied, where $\sigma$ is out-of-plane strain defined by $(d\text{-}c_0)/c_0$ with $d$=$c$ for (001)-films and $d_{110}/\sqrt{2}$ for (110)-films. In Fig. 4c we present the representative $M_S$-$\sigma$ relations for the LCO and LSCO($x$=0.2) films. From a first sight, all data of the LCO films collapse into a master curve, ascending monotonically from ~0.1 to ~0.9 $\mu_B$/Co as $d$ decreases from ~-0.82% to ~1.77%. According to this $M_S$-$\sigma$ relation, the $M_S$ increasingly increases towards the low $\sigma$ limit, and $M_S$ values well beyond 1 $\mu_B$/Co are available if further strain is achievable. In contrast, the LSCO films exhibit a much more complex behavior: With the increase of $d$, $M_S$ first increases and then decreases, yielding a local maximum of ~1 $\mu_B$/Co around $\sigma$=0. Different from LCO, 1 $\mu_B$/Co is the highest value that can be invoked by simply adjusting lattice strains. Assuming that all of the $Co^{4+}$ ions are in the LS state while half $Co^{3+}$ ions in the IS and half $Co^{3+}$ ions in the LS state, a simple calculation gives $M_S$=0.2 × 1+2 × 0.4=1 $\mu_B$/Co, where the Lander's $g$-factor has been set to 2.

Based on the data in Figs. 3 and 4, we obtained the phase diagrams in Fig. 5. Figs. 5a and 5c show the phase distribution on the *T-x* plane for the LSOC/STO and LSCO/LAO films, respectively. Presence of a NM window ($0.1 < x < 0.2$) in the former films and the enhanced FM character with $x$ in the latter films can be clearly seen. Sandwiched by these two figures is a mapping of $M_S$ on the σ-$x$ plane (Fig. 5b), derived from the $M_S$-$\sigma$ relations of different Sr contents. The most remarkable feature is the existence of a downwards curved NM strip, where $M_S$ is low (blue-colored region). It demonstrates the depression of lattice strain on the FM state. Take the case of tensile strain as an example (it corresponds to out-of-plane compressive strain). The NM window can even go deep into the doping range ($x$>0.2) where the DE prevails in bulk LSCO. From this phase diagram, we would expect a magnetic switching whenever a deviation from strain-free state occurs for LSCO of $x > 0.1$. The increased magnetization at the

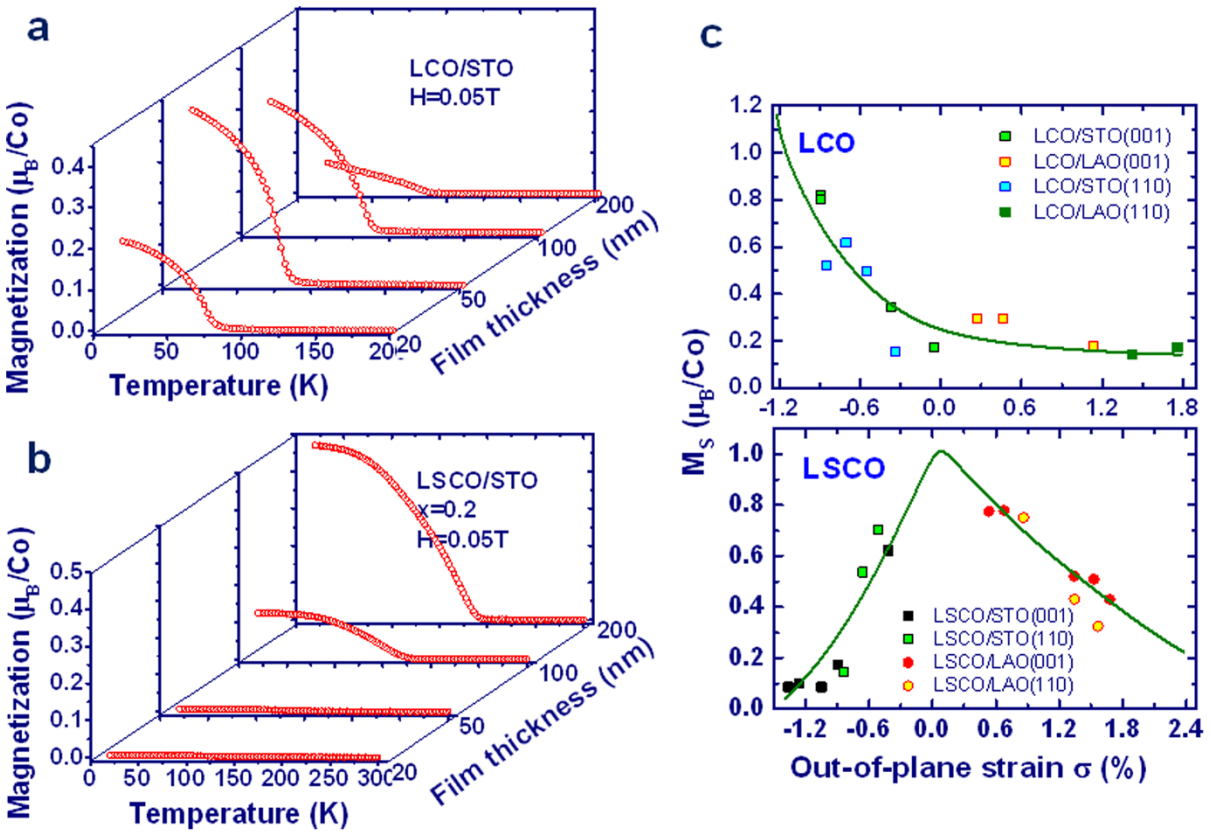


**Figure 4 | Strain effect on magnetism for the LSCO films grown on different substrates, with the strains being tuned by film thickness.** (a) and (b) Temperature-dependent magnetization of the LSCO/STO film with different thicknesses, recorded in the warming process after field cooling the films to 10 K. (a) and (b) correspond to x=0 and 0.2, respectively. The applied field is 0.05 T. (c) Saturation magnetization as a function of out-of-plane lattice strain (σ), extracted from the M-H curves recorded at 10 K. The top and bottom panels correspond to the LCO and LSCO(x=0.2) films, respectively. Solid lines are guides for the eye.

lower left counter of this σ-*x* plane is an exception, where the SE prevails.

***Ab initio* calculation of magnetic property.** To get a further understanding of the distinctive doping effects, we performed *ab initio* calculations on the magnetic property of LSCO within the framework of density functional theory. As shown by the green symbols in Figs. 3e and 3f, the calculated magnetic moments satisfactorily reproduce the trends in the experimental data, i.e., the dramatic reduction of $M_S$ in intermediate doping range in LSCO/STO and the monotonic $M_S$ growth in LSCO/LAO, indicating that the theoretical model has captured the main features of the strained effect.

To quantify structural features, we analyzed the atomic configurations around Sr in the supercells. For the LCO/STO film, the $CoO_6$

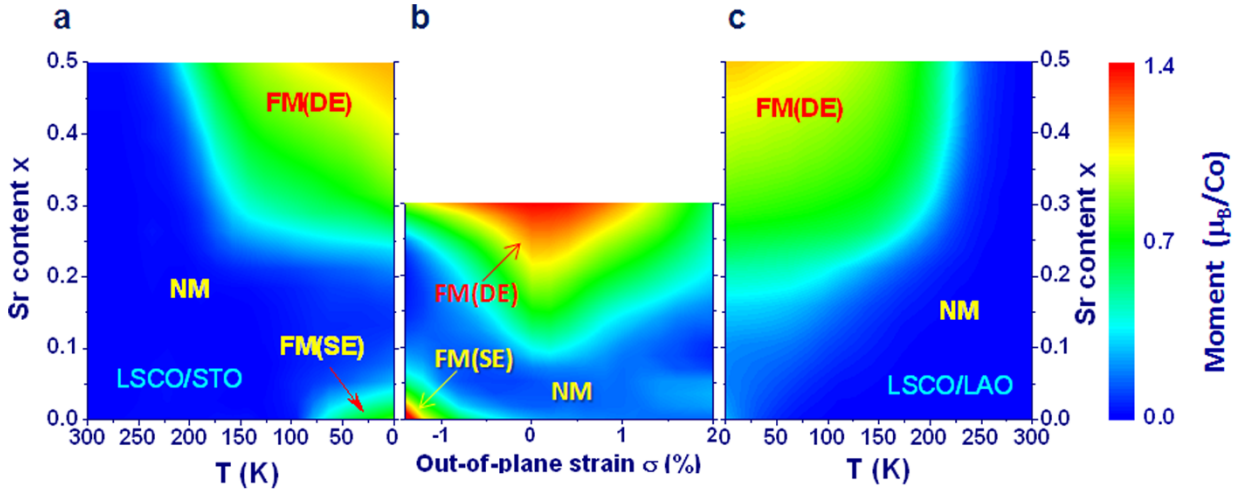


**Figure 5 |** Phase diagram on the *T*-*x* plane of LSCO films grown above STO (a) and LAO (c). (b) Distribution of saturation magnetization on the σ-*x* plane. Labels "FM(SE)" and "FM(DE)" denote the FM phases mediated by superexchange and double exchange, respectively. "NM" denotes nonmagnetic or paramagnetic phase.

polyhedron deviates considerably from the octahedral symmetry. Due to the presence of tensile strains, in-plane and out-of-plane Co-O bonds are significantly different. As illustrated in Fig. 6a, two $CoO_6$ octahedra in the supercell of LCO are elongated while other two compressed along the *z*-axis. A direct calculation indicates that the $Co^{3+}$ ion in the more severely elongated $O_6$ cage is in the HS state (marked by light cyan color) while other three $Co^{3+}$ ions are in the LS state. This ratio is lower than that deduced from the data of x-ray absorption spectroscopy[25] but well agrees with the observation that $M_S$ is ~1 $\mu_B$/Co. The distortion of the $CoO_6$ octahedron has influenced the electronic population of the $t_{2g}$ and $e_g$ levels, stabilizing the HS state. As established, the SE between HS-LS-HS $Co^{3+}$ ions gives rise to the FM order in tensile LCO film[14,19].

Fig. 6b presents the projected density of states for 3*d* orbitals at a LS $Co^{3+}$ site (left panel) and a HS $Co^{3+}$ site (right panel) of the LCO/STO film. As expected, spin-up and spin-down states display different densities for HS $Co^{3+}$ but similar densities for LS $Co^{3+}$. As shown in Fig. 5c, the two elongated $CoO_6$ polyhedrons at $x$=0 disappear after the doping of $x$=0.125. According to the 1 : 3 HS to LS $Co^{3+}$ ratio, on average each $La^{3+}$ in LCO/STO will have two HS $Co^{3+}$ and six LS $Co^{3+}$ neighbors. Due to their large $CoO_6$ cell volume, the two HS $Co^{3+}$ ions (marked by light cyan color) will be the first ones to be affected by Sr, being transited into LS $Co^{4+}$ and LS $Co^{3+}$, respectively. Here $Co^{4+}$ and $Co^{3+}$ appear as LS ions to vacate space for $Sr^{2+}$ that is larger than $La^{3+}$. After a simple calculation, we obtain an equation for magnetization, $M_S$=(1-7$x$) $\mu_B$/Co. According to this equation, HS $Co^{3+}$ ions will completely disappear at $x$~0.15, which is exactly in the middle of the NM window. With the help of lattice strain, the incorporation of Sr has promoted the population of $Co^{3+}$ in the LS state. This is in sharp contrast to the doping effect on bulk LCO, which transits LS $Co^{3+}$ into IS $Co^{3+}$. Obviously, doping effect has gained new features in the presence of lattice strain. Due to the clamping of the substrate, Sr affects not only the transited $Co^{4+}$ ion but also a neighboring HS $Co^{3+}$ ion, greatly depressing both the SE and the DE

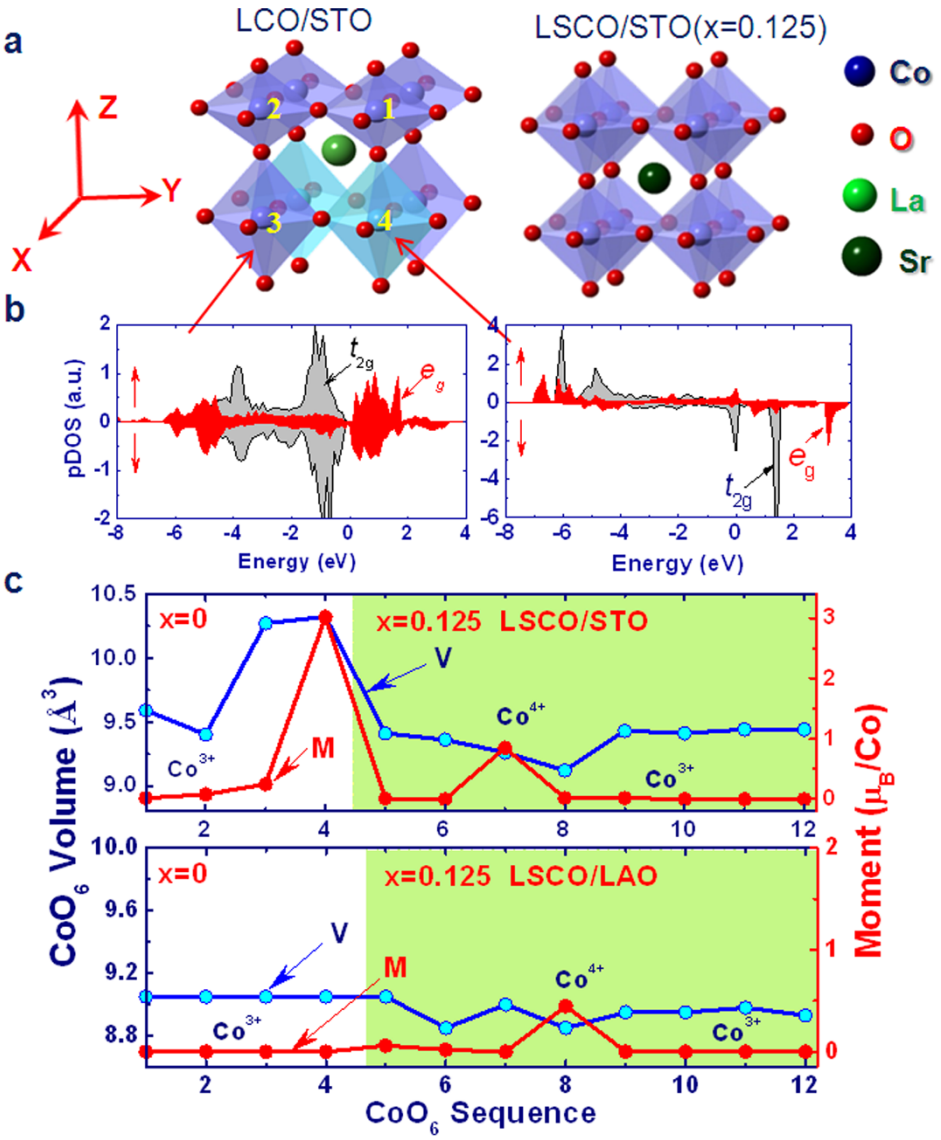


**Figure 6** | (a) Schematic diagram of the distorted $CoO_6$ polyhedrons in LCO/STO. Number besides octahedron indicates its sequence in supercell. Light cyan marks the $CoO_6$ octahedron in the HS state. After the incorporation of Sr, the two HS $Co^{3+}$ in elongated $CoO_6$ octahedra (light cyan) are transited into a LS $Co^{3+}$ and a LS $Co^{4+}$ state, respectively. Meanwhile, the $CoO_6$ octahedra reshape to accommodate the structure deformation thus resulted. (b) Projected density of states for 3*d* orbitals at a LS $Co^{3+}$ site (left panel) and a HS $Co^{3+}$ site (right panel) for the marked $CoO_6$ octahedra in (a). Dashed line marks the Fermi energy. The positive and negative densities of states are for spin up and spin down, respectively. (c) Cell volume of the $CoO_6$ octahedra in the supercells and the magnetic moment of the Co ions in the $O_6$ cages, numbed in sequence. "M" and "V" denote magnetic moment and cell volume, respectively.

interactions. When $x$ is high, the strain effect is partially overcome by enhanced DE. Due to cooperative lattice distortions, Sr doping now favors an IS state rather than simply depresses the spin state of $Co^{3+}$, causing a magnetic upturn of the $M_S$-$x$ curve (Fig. 1e).

For the LCO/LAO film, the $CoO_6$ polyhedron is nearly perfectly octahedral. This implies a high degeneracy of the $t_{2g}$ orbits and the $e_g$ orbits, thus the $Co^{3+}$ ions are mainly in the LS state. It explains the low $M_S$ of LCO/LAO. Our LCO/LAO film shows a finite $M_S$, probably due to the presence of cation vacancies which give rise to native $Co^{4+}$ ions. The introduction of Sr at least will transit a LS $Co^{3+}$ into a LS $Co^{4+}$ (see the case of when $x$ =0.125 in the bottom panel of Fig. 6c), assigning Co ions magnetic moments. Consequently, $M_S$ grows monotonically with $x$. We note that the Jahn-Teller-like distortion of the $CoO_6$ octahedron in LSCO/LAO of $x$=0.125 is obviously weaker than that in corresponding LSCO/STO; the in-plane and out-of-plane Co-O bond ratio is ~1% for LSCO/LAO and ~5% for LSCO/STO. It may explain the weakness of the strain effect in LSCO/LAO.

In conclusion, tensile strain favors the FM state of LCO but strongly destabilizes the FM state of LSCO, and even generates a NM window that embeds deep into the doping range of the FM phase in bulk counterparts. *Ab initio* calculations indicate that, with the help of lattice strain, the introduction of Sr triggers a high to low spin state transition for the $Co^{3+}$ ions. This, together with strain-enhanced Jahn-Teller distortions, weakens the FM coupling between $Co^{3+}$ and $Co^{4+}$, leading to the NM window. Compared with tensile strain, the effect of compressive strain is slightly weak, thanks to reduced Jahn-Teller distortion.

## Methods

**Sample fabrication.** $La_{1-x}Sr_xCoO_3$ films with a Sr content between 0 and 0.5 were grown respectively on (001) and (110)-orientated $LaAlO_3$ and $SrTiO_3$ substrates ($3 \times 5 \times 0.5$ $mm^3$) using pulsed laserablation technique ($\lambda$=248 nm). The fluence of the laser pulses was 1.5 $J/cm^2$, and the repetition rate was 1 Hz. In deposition process, the substrate was kept at 800°C and the oxygen pressure at 50 Pa. The film thickness, $t$, varies between 20 nm and 200 nm, determined by the deposition time. After deposition, the films were *in-situ* annealed for 15 min in an $O_2$ pressure of 1 bar before cooling down to the ambient temperature.

**Structural and magnetic characterizations.** Morphology of the film was analyzed by the atomic force microscopy (Seiko SPI 3800N) at the ambient conditions. The crystal structure of the films was determined by a Bruker diffractometer equipped with thin film accessories (D8 Discover, $\lambda$ = 1.5406 Å). High-resolution aberration-corrected scanning transmission electron microscopy (STEM) investigation was carried out on a JEM-ARM200F microscope with double $C_S$ correctors for the condenser lens and objective lens. The available point resolution is better than 0.08 nm at an operating voltage of 200 kV. The high angle annular dark-field (HAADF) images were acquired at acceptance angles of 70–150 mrad. Magnetic measurements were conducted on a Quantum Design vibrating sample magnetometer (VSM-SQUID) in the temperature interval from 5 to 300 K.

**Density functional theory calculations.** The projector augmented plane-wave (PAW) pseudo-potentials were used, as implemented in the Vienna *ab-initio* Simulation Package (VASP). To accurately describe exchange and correlation interactions, the local spin density approximation (LSDA)+U method[26,27] was employed with the effective Hubbard parameter of $U_{eff}$=3.8 eV for Co in LCO, and $U_{eff}$=3.3 eV for Co in Sr doped LCO, referring to Ref. 19. The supercells adopted in the calculation are $\sqrt{2}a_0 \times \sqrt{2}a_0 \times 2a_0$, $\sqrt{2}a_0 \times \sqrt{2}a_0 \times 4a_0$, $\sqrt{2}a_0 \times \sqrt{2}a_0 \times 5a_0$, $\sqrt{2}a_0 \times \sqrt{2}a_0 \times 3a_0$, and $\sqrt{2}a_0 \times \sqrt{2}a_0 \times 2a_0$ for the Sr concentration of 0, 0.125, 0.2, 0.33, and 0.5, respectively, where $a_0$ is the bulk lattice constant of the perovskite unit cell. A brief description of the calculation procedure is as follows. First, a stable and strain-free structure is established for LSCO through optimizing the total energy of the system, and the resulted lattice was expanded along in-plane direction to fit the experimental one. Second, the resulting lattice was subjected to an adjustment along out-of-plane direction to get an energy minimum. For this state, the electronic and magnetic structures are calculated.


1. Itoh, M., Natori, I., Kubota, S. & Motoya, K. Spin-glass behavior and magnetic phase diagram of $La_{1-x}Sr_xCoO_3$ ($0 \le x \le 0.5$) studied by magnetization measurements. *J. Phys. Sco. Jpn.* **63**, 1486–1493 (1994).
2. Señarís-Rodríguez, M. A. & Goodenough, J. B. Magnetic and transport properties of the system $La_{1-x}Sr_xCoO_3$ ($0 < x \le 0.5$). *J. Solid State Chem.* **118**, 232–336 (1995).
3. Tokura, Y., Okimoto, Y., Yamaguchi, S. & Taniguchi, H. Thermally induced insulator-metal transition in $LaCoO_3$: A view based on the Mott transition. *Phys. Rev. B* **58**, 1699–1702 (R) (1995).
4. Korotin, M. A. *et al.* Intermediate-spin state and properties of $LaCoO_3$. *Phys. Rev.* B **54**, 5309–5316 (1996).
5. Saitoh, T. *et al.* Electronic structure and temperature-induced paramagnetism in $LaCoO_3$. *Phys. Rev. B* **55**, 4257–4266 (1997).
6. Ishikawa, A., Nohara, J. & Sugai, S. Raman Study of the Orbital-Phonon Coupling in $LaCoO_3$. *Phys. Rev. Lett.* **93**, 136401 (2004).
7. Haverkort, M. W. *et al.* Spin state transition in $LaCoO_3$ studied using soft x-ray absorption spectroscopy and magnetic circular dichroism. *Phys. Rev. Lett.* **97**, 176405 (2006).
8. A. Podlesnyak A. *et al.* Spin incommensurability and two phase competition in cobaltites. *Phys. Rev. Lett.* **97**, 247208 (2006).
9. Hong, W. T. *et al.* Tuning the spin state in $LaCoO_3$ thin films for enhanced high-temperature oxygen electrocatalysis. *Phys. Chem. Lett.* **4**, 2493 (2013).
10. Fuchs, D. *et al.* Ferromagnetic order in epitaxially strained $LaCoO_3$ thin films. *Phys. Rev. B* **75**, 144402 (2007).
11. Fuchs, D. *et al.* Tuning the magnetic properties of LaCoO3 thin films by epitaxial strain. *Phys. Rev. B* **77**, 014434 (2008).
12. Fuchs, D. *et al.* Suppression of the ferromagnetic state in LaCoO3 films by rhombohedral distortion. *Phys. Rev. B* **79**, 024424 (2009).
13. Choi, W. S. *et al.* Strain-induced spin states in atomically ordered cobaltites. *Nano Lett.* **12**, 4966–4970 (2012).
14. Merz, M. *et al.* X-ray absorption and magnetic circular dichroism of $LaCoO_3$, $La_{0.7}Ce_{0.3}CoO_3$, and $La_{0.7}Sr_{0.3}CoO_3$ films: Evidence for cobalt-valence-dependent magnetism. *Phys. Rev. B* **82**, 174416 (2010).
15. Fujioka, J. *et al.* Spin-orbital superstructure in strained ferrimagnetic perovskite cobalt oxide. *Phys. Rev. Lett.* **111**, 027206 (2013).
16. Fuchs, D. *et al.* Double exchange via $t_{2g}$ orbitals and the Jahn-Teller effect in ferromagnetic $La_{0.7}Sr_{0.3}CoO_3$ probed by epitaxial strain. *Phys. Rev. Lett.* **111**, 257203 (2013).
17. Biškup, N. *et al.* Insulating ferromagnetic $LaCoO_{3-\delta}$ films: a phase induced by ordering of oxygen vacancies. *Phys. Rev. Lett.* **112**, 087202 (2014).
18. Hu, C. *et al.* Voltage-controlled ferromagnetism and magnetoresistance in $LaCoO_3/SrTiO_3$ heterostructures. *J. Appl. Phys.* **114**, 183909 (2013).
19. Seo, H., Posadas, D. & Demkov, A. A. Strain-driven spin-state transition and superexchange interaction in $LaCoO_3$: *Ab initio* study. *Phys. Rev. B* **86**, 014430 (2012).
20. Rata, A. D., Herklotz, A., Nenkov, K., Schultz, L. & Dörr, K. Strain-induced insulator state and giant gauge factor of $La_{0.7}Sr_{0.3}CoO_3$ films. *Phys. Rev. Lett.* **100**, 076401 (2008).
21. Xie, C. K., Budnick, J. I., Hines, W. A., Wells, B. O. & Woicik, J. C. Strain-induced change in local structure and its effect on theferromagnetic properties of $La_{0.5}Sr_{0.5}CoO_3$ thin films. *Appl. Phys. Lett.* **93**, 182507 (2008) .
22. Caciuffo, R. *et al.* Structural details and magnetic order of $La_{1-x}Sr_xCoO_3$ ($x \le 0.3$). *Phys. Rev. B* **59**, 1068–1078 (1999).
23. Choi, W. S. *et al.* Strain-induced spin states in atomically ordered cobaltites. *Nano Lett.* **12**, 4966–4970 (2012).
24. Biškup, N. *et al.* Insulating ferromagnetic $LaCoO_{3-\delta}$ films: a phase induced by ordering of oxygen vacancies. *Phys. Rev. Lett.* **112**, 087202 (2014).
25. Pinta, C. *et al.* Suppression of spin-state transition in epitaxially strained $LaCoO_3$. *Phys. Rev. B* **78**, 174402 (2008).
26. Anisimov, V. I., Zaanen, J. & Andersen, O. K. Band theory and Mott insulators-Hubbard-u instead of Stoner-I. *Phys. Rev. B* **44**, 943–954 (1991).
27. Anisimov, V. I. *et al.* Density -functional theory and NiO photoemission spectra. *Phys. Rev. B* **48**, 16929–16934 (1993).


## Acknowledgments

This work has been supported by the National Basic Research of China (Grant Nos. 2011CB921801, 2012CB921403, and 2013CB921701) and the National Natural Science Foundation of China (Grant Nos. 11074285, 51372064, and 11134007).

## Author contributions

J.R.S. conceived and designed the experiments, analyzed and interpreted the data. H.W.Y. and H.R.Z. prepared the samples, preformed the structural and magnetic measurements and, together with S.F.W., primarily analyzed the experimental data. H.W.Y. and S.M. conducted the first-principle calculation. The AFM characterizations of the sample were made by Y.L. The transmission electron microscope analysis was conducted by X.S., Q.Q.L. and R.C.Y. J.R.S. wrote the manuscript. B.G.S. oversaw the project. All authors commented on the manuscript.

## Additional information

**Competing financial interests:** The authors declare no competing financial interests.

**How to cite this article:** Yang, H.W. *et al.* Anomalous magnetism in strained $La_{1-x}Sr_xCoO_3$ epitaxial films ($0 \le x \le 0.5$). *Sci. Rep.* **4**, 6206; DOI:10.1038/srep06206 (2014).